Ghenadii Korotcenkov *Editor*

Handbook of II-VI Semiconductor-Based Sensors and Radiation Detectors

Vol. 3: Sensors, Biosensors and Radiation Detectors

Springer

Handbook of II-VI Semiconductor-Based Sensors and Radiation Detectors

Ghenadii Korotcenkov
Editors

Handbook of II-VI Semiconductor-Based Sensors and Radiation Detectors

Vol. 3: Sensors, Biosensors and Radiation Detectors

Springer

Editor
Ghenadii Korotcenkov
Department of Physics and Engineering
Moldova State University
Chisinau, MD-2009, Moldova

ISBN 978-3-031-23999-1 ISBN 978-3-031-24000-3 (eBook)
https://doi.org/10.1007/978-3-031-24000-3

This Springer imprint is published by the registered company Springer Nature Switzerland AG
The registered company address is: Gewerbestrasse 11, 6330 Cham, Switzerland

Preface

Binary and ternary semiconductors of II–VI group (ZnS, ZnSe, ZnTe, CdS, CdSe, CdTe, HgTe, HgS, HgSe, HgCdTe, CdZnTe, CdSSe and HgZnTe) are very popular among researchers because of their remarkable physical and chemical properties, which, as a group, are unique. II–VI compounds possess a very wide spectrum of electronic and optical properties. Most materials of group II–VI are semiconductors with a direct band gap and high optical absorption and emission coefficients. In addition, binary II–VI compounds are easily miscible, providing a continuous range of properties. As a result, the II–VI semiconductors possess band gap, varying over a wide range. Therefore, II–VI compounds can serve as efficient light emitters such as light diodes and lasers, solar cells, and radiation detectors operated in the range from IR to UV and X-ray. II–VI compound-based devices can also cover terahertz range. Besides common photovoltaic applications, II–VI semiconductors are also potential candidates for a variety of electronic, electro-optical, sensing and piezoelectric devices. In particular, nanoparticles of II–VI semiconductors, such as quantum dots, one-dimensional structures and core-shells structures, can be used for the development of gas sensors, electrochemical sensors and biosensors. These semiconductors, when downsized to nanometer, have become the focus of attention because of their tunable band structure, high extinction coefficient, possible multiple exciton generation and unique electronic and transport properties. It is important that II–VI semiconductors can be easily prepared in high-quality epitaxial, polycrystalline and nanocrystalline films. The concentration of charge carriers can also vary in II–VI semiconductors in a wide range due to doping. Thus, the use of II–VI films represents an economical approach to the synthesis of semiconductors for various applications. It should be noted that the range of technical applications for II–VI compounds goes beyond the better-known semiconductors such as Si, Ge and some of the III–V compounds.

Formally, metal oxides such as CdO and ZnO also belong to II–VI compounds. However, we will not cover them in this book. In recent years, these compounds have been allocated to a separate group “Metal oxides,” and many books have been devoted to their discussion, in contrast to other II–VI compounds. In particular, for

those who are interested in exactly these compounds, we can recommend the *Metal Oxides* series which is published by Elsevier.

The aim of this three-volume book is to provide an updated account of the state of the art of multifunctional II–VI semiconductors, from fundamental sciences and material sciences to their applications as various sensors and radiation detectors, and, based on this knowledge, to formulate new goals for further research. The proposed book provides an interdisciplinary discussion of a wide range of topics, such as synthesis of II–VI compounds, their deposition, processing, characterization, device fabrication and testing. Topics of the recent remarkable progresses in the application of nanoparticles, nanocomposites and nanostructures consisting of II–VI semiconductors in various devices are also covered. Both experimental and theoretical approaches were used for this analysis.

Currently, there are already published books on II–VI semiconductors. However, some of them were published too long ago and they cannot reflect the current state of research in this area. Other published books focus on a limited number of topics, from which topics related to various sensor applications such as gas sensors, humidity sensors and biosensors are almost completely excluded. When considering photodetectors, the focus is also only on the analysis of IR photodetectors. However, sensors operated in the visible, ultraviolet and X-ray ranges also hold great promise for applications. With these books, we will try to close this gap.

Proposed our three-volumes book *Handbook of II–VI Semiconductor-Based Sensors and Radiation Detectors* is the first to cover both chemical sensors and biosensors and all types of photodetectors and radiation detectors based on II–VI semiconductors. It contains a comprehensive and detailed analysis of all aspects of the application of II–VI semiconductors in these devices. This makes these books very useful and comfortable to use. Combining this information in three volumes, united by common topics, should help readers in finding the necessary information on the required subject.

Chapters in *Handbook of II–VI Semiconductor-Based Sensors and Radiation Detectors. Vol. 1: Materials and Technologies* describe the physical, chemical and electronic properties of II–VI compounds, which give rise to an increased interest in these semiconductors. Technologies that are used in the development of various devices based on II–VI connections are also discussed in detail in this volume.

Handbook of II–VI Semiconductor-Based Sensors and Radiation Detectors. Vol. 2: Photodetectors focuses on the consideration of all types of optical detectors, including IR detectors, visible and UV detectors. This consideration includes both the fundamentals of the operation of detectors and the peculiarities of their manufacture and use. An analysis of new trends in the development of II–VI semiconductors-based photodetectors is also given.

Handbook of II–VI Semiconductor-Based Sensors and Radiation Detectors. Vol. 3: Sensors, Biosensors and Radiation Detectors describes the use of II–VI compounds in other fields such as radiation detectors, gas sensors, humidity sensors, optical sensors and biosensors. The chapters in this volume provide a comprehensive overview of the manufacture, parameters and applications of these devices.

We believe that these books will enable the reader to understand the present status of II–VI semiconductors and their role in the development of a new generation of photodetectors, chemical sensors, biosensors and radiation detectors. I am very pleased that many well-known experts with extensive experience in the development and research of II–VI semiconductor sensors and radiation detectors were involved in the preparation of the chapters of these books.

The target audience for this series of books are scientists and researchers working or planning to work in the field of materials related to II–VI semiconductors, i.e. scientists and researchers whose activities are related to electronics, optoelectronics, chemical and biosensors, electrical engineering, biomedical applications, etc. I believe this three-volume book may also be of interest to practicing engineers or project managers in industries and national laboratories who would like to develop II–VI semiconductor-based photodetectors, radiation detectors and sensors but do not know how to do it, and how to select the optimal II–VI semiconductor for specific applications. With numerous references to an extensive resource of recently published literature on the subject, these books can serve as an important and insightful source of valuable information, providing scientists and engineers with new ideas for understanding and improving existing II–VI semiconductor devices.

I believe that these books will be very useful for university students, doctoral students and professors. The structure of these books offers the basis for courses in materials science, chemical engineering, electronics, optoelectronics, environmental control, chemical sensors, photodetectors, radiation detectors, biomedical applications and many others. Graduate students may also find the book very useful in their research and understanding of the synthesis of II–VI semiconductors, study and application of this multifunctional material in various devices. We are confident that all of them will find the information useful for their activities.

Finally, I thank all the authors who contributed to these books. I am grateful that they agreed to participate in this project and for their efforts to prepare these chapters. This project would not have been possible without their participation. I am also very grateful to Springer for the opportunity to publish this book with their help. I would also like to inform that my activity related to editing this book was funded by the State Program of the Republic of Moldova project 20.80009.5007.02.

I am also grateful to my family and wife, who always support me in all my endeavors.

Chisinau, Moldova Ghenadii Korotcenkov

Contents

Part I X-Ray Radiation Detectors

1 Basic Principles of Solid-State X-Ray Radiation Detector Operation 3
M. Zahangir Kabir

2 CdTe-/CdZnTe-Based Radiation Detectors 35
A. Opanasyuk, D. Kurbatov, Ya. Znamenshchykov, O. Diachenko, and M. Ivashchenko

3 ZnS-Based Neutron and Alpha Radiation Detectors 75
Ghenadii Korotcenkov and Michail Ivanov

4 ZnSe- and CdSe-Based Radiation Detectors 109
Shweta Jagtap, Madhushree Bute, Sapana Rane, and Suresh Gosavi

5 Medical Applications of II-VI Semiconductor-Based Radiation Detectors 137
Ghenadii Korotcenkov and Sergiu Vatavu

Part II Electric and Electronic Chemical Sensors

6 Introduction in Gas Sensing 161
Ghenadii Korotcenkov and Vladimir Brinzari

7 II-VI Semiconductor-Based Thin Film Electric and Electronic Gas Sensors 177
Stella Vallejos and Chris Blackman

8 Nanocomposite and Hybrid-Based Electric and Electronic Gas Sensors 201
Roman B. Vasiliev, Artem S. Chizhov, and Marina N. Rumyantseva

9 II–VI Semiconductor-Polymer Nanocomposites and Their Gas-Sensing Properties 233
Chandan Kumar, Satyabrata Jit, Sumit Saxena, and Shobha Shukla

10 Nanomaterial-Based Electric and Electronic Gas Sensors 253
Andrea Gaiardo, Barbara Fabbri, and Matteo Valt

11 II–VI Semiconductor-Based Humidity Sensors 281
Ghenadii Korotcenkov, Michail Ivanov, and Vladimir Brinzari

Part III Optical Sensors

12 II–VI Semiconductor-Based Optical Gas Sensors 307
Savita Sharma, Ayushi Paliwal, Pragati Kumar, and Nupur Saxena

13 Spectroscopic Gas Sensing Systems 335
Zhenhui Du and Jinyi Li

14 Luminescence and Fluorescence Ion Sensing 361
Faheem Amin, Yasir Iqbal, and Ghenadii Korotcenkov

15 Photoelectrochemical Ion Sensors 393
Alka Pareek and Pramod H. Borse

16 II–VI Semiconductor-Based Optical Temperature Sensors 417
Nupur Saxena and Pragati Kumar

Part IV Biosensors

17 Introduction to Biosensing 441
Ghenadii Korotcenkov, Rabiu Garba Ahmad, Praveen Guleria, and Vineet Kumar

18 Fluorescent Biosensors Based on II–VI Quantum Dots 475
Nguyen Thu Loan, Ung Thi Dieu Thuy, and Nguyen Quang Liem

19 QDs-Based Chemiluminescence Biosensors 509
Fahimeh Ghavamipour and Reza H. Sajedi

20 Electrochemiluminescent Biosensors Based on II–VI Quantum Dots 531
Xiao-Yan Wang, Zhi-Yuan Che, and Shou-Nian Ding

21 Electrochemical Biosensors 551
Mayank Garg, Arushi Gupta, Amit L. Sharma, and Suman Singh

22 Photoelectrochemical Biosensors 567
Sirlon F. Blaskievicz, Byanca S. Salvati, Alessandra Alves Correa, and Lucia Helena Mascaro

23 II–VI Semiconductor QDs in Surface Plasmon Resonance Sensors . 589
Hina F. Badgujar and Anuj K. Sharma

24 Biomarkers and Bioimaging and Their Applications 615
Suchismita Ghosh and Kaustab Ghosh

25 Biosensors Based on II–VI Semiconductor Quantum Dots for Health Protection 633
Suria Mohd Saad and Jaafar Abdullah

26 Application of II–VI Semiconductor-Based Biosensors in Nanomedicine and Bioanalysis 653
Bruno Gabriel Lucca and Jacqueline Marques Petroni

27 Specific Applications of II–VI Semiconductor Nanomaterials-Based Biosensors for Food Analysis and Food Safety 673
Xiaodong Guo, Jiaqi Wang, Mengke Zhang, and Marie-Laure Fauconnier

Index 697

About the Editor

Ghenadii Korotcenkov received his PhD in physics and technology of semiconductor materials and devices in 1976 and his doctor of science degree (doctor habilitate) in physics of semiconductors and dielectrics in 1990. He has more than 50-year experience as a teacher and scientific researcher. Long time he was a leader of gas sensor group and manager of various national and international scientific and engineering projects carried out in the Laboratory of Micro- and Optoelectronics, Technical University of Moldova, Chisinau, Moldova. International foundations and programs such as the CRDF, the MRDA, the ICTP, the INTAS, the INCO-COPERNICUS, the COST and NATO have supported his research. From 2007 to 2008, he carried out his research as an invited scientist in Korea Institute of Energy Research (Daejeon). Then, from 2008 to 2018, Dr. G. Korotcenkov was a research professor in the School of Materials Science and Engineering at Gwangju Institute of Science and Technology (GIST) in Korea. Currently, G. Korotcenkov is a chief scientific researcher at Moldova State University, Chisinau, Moldova.

Scientists from the former Soviet Union know the results of G. Korotcenkov's research in the study of Schottky barriers, MOS structures, native oxides and photoreceivers based on III–Vs compounds such as InP, GaP, AlGaAs and InGaAs. His current research interests since 1995 include material sciences, focusing on metal oxide film deposition and characterization (In_2O_3, SnO_2, ZnO, TiO_2), surface science, thermoelectric conversion and design of physical and chemical sensors, including thin film gas sensors.

G. Korotcenkov is the author or editor of 45 books and special issues, including 11-volume *Chemical Sensors* series published by Momentum Press, two-volumes *Handbook of Gas Sensor Materials* published by Springer, 15-volume *Chemical Sensors* series published by Harbin Institute of Technology Press, China, three-volumes *Porous Silicon: From Formation to Application* issue published by CRC

Press, three-volumes *Handbook of Humidity Measurements* published by CRC Press, three-volumes *Handbook of II-VI Semiconductor-based Sensors and Radiation Detectors* published by Springer, and 6 proceedings of the international conferences published by Trans Tech Publ., Elsevier and EDP Sciences. In addition, currently he is a series editor of *Metal Oxides* book series published by Elsevier. Since 2017, more than 35 volumes have been published within this series.

G. Korotcenkov is the author and coauthor of more than 675 scientific publications, including 34 review papers, 62 book chapters, more than 200 peer-reviewed articles published in scientific journals (h-factor = 43 (Web of Science), h = 45 (Scopus) and h = 60 (Google scholar citation), 2022). He is the holder of 17 patents. He presented more than 250 reports on national and international conferences, including 17 invited talks. G. Korotcenkov, as a cochairman or member of program, scientific and steering committees, has participated in the organization of more than 40 international scientific conferences. Dr. G. Korotcenkov is a member of editorial boards in five scientific international journals. His name and activities have been listed by many biographical publications including Who's Who. G. Korotcenkov have also been listed as one of the "World's Ranking Top 2% Scientists" in Applied Physics/Analytical Chemistry in the Physics and Astronomy Cluster. His research activities have been honored by the National Prize of the Republic of Moldova (2022), the Honorary Diploma of the Government of the Republic of Moldova (2020), an Award of the Academy of Sciences of Moldova (2019), an Award of the Supreme Council of Science and Advanced Technology of the Republic of Moldova (2003); the Prize of the Presidents of the Ukrainian, Belarus, and Moldovan Academies of Sciences (2004); Senior Research Excellence Award of Technical University of Moldova (2001; 2003; 2005), the National Youth Prize of the Republic of Moldova in the field of science and technology (1980), among others. Some of his research results and published books have won awards at international exhibitions. G. Korotcenkov also received fellowships from the International Research Exchange Board (IREX, United States, 1998), Brain Korea 21 Program (2008–2012) and BrainPool Program (Korea, 2007–2008 and 2015–2017).https://www.scopus.com/authid/detail.uri?authorId=6701490962https://publons.com/researcher/1490013/ghenadii-korotcenkov/https://scholar.google.com/citations?user=XR3RNhAAAAAJ&hlhttps://www.researchgate.net/profile/G_Korotcenkov

Part I
X-Ray Radiation Detectors

Chapter 1
Basic Principles of Solid-State X-Ray Radiation Detector Operation

M. Zahangir Kabir

1.1 Introduction

X-rays are electromagnetic waves, whose photon energies range roughly from 0.1 keV to 125 keV. The X-rays are classified as soft X-rays (from 0.1 keV to 10 keV) and hard X-rays (10 keV to 125 keV). X-rays are used in various types of imaging purposes; for examples, diagnostic medical X-ray imaging cover photon energies from 10 keV up to 120 keV, crystallography uses X-ray photons of energy around 10 keV, security scanning uses photon energies from 80 to 140 keV, and X-ray microscopy and fluorescence spectroscopy cover photon energies ranging from 0.1 to 3 keV, as shown in Fig. 1.1. Different applications require different specialized detectors having different suitable photoconductors and detector designs.

A radiation detector is a device that converts the energy (or part of the energy) of the incident radiation into a measurable electrical signal. In other words, it can measure the presence of a particular type of radiation. There are two types of X-ray detectors: (1) scintillation detectors and (2) solid-state semiconductor detectors. In scintillator detectors, X-ray energy is converted into light photons in the scintillator layer and these light photons are then detected by a photodetector. In solid-state semiconductor detectors (also known as the direct conversion detector), X-ray photons directly generate electron and hole pairs (EHPs) in the photoconductor layer, which are collected on electrodes. Semiconductor X-ray radiation detectors are the most important class of detectors for detecting and measuring this type of radiation because of their solid-state structure, higher resolution, and efficiency. These semiconductor radiation detectors are also used as imaging detectors and capture X-ray images by arranging them in arrays. A simplified functional classification of

M. Z. Kabir (✉)
Department of Electrical and Computer Engineering, Concordia University, Montreal, QC, Canada
e-mail: zahangir.kabir@concordia.ca

G. Korotcenkov (ed.), *Handbook of II-VI Semiconductor-Based Sensors and Radiation Detectors*, https://doi.org/10.1007/978-3-031-24000-3_1

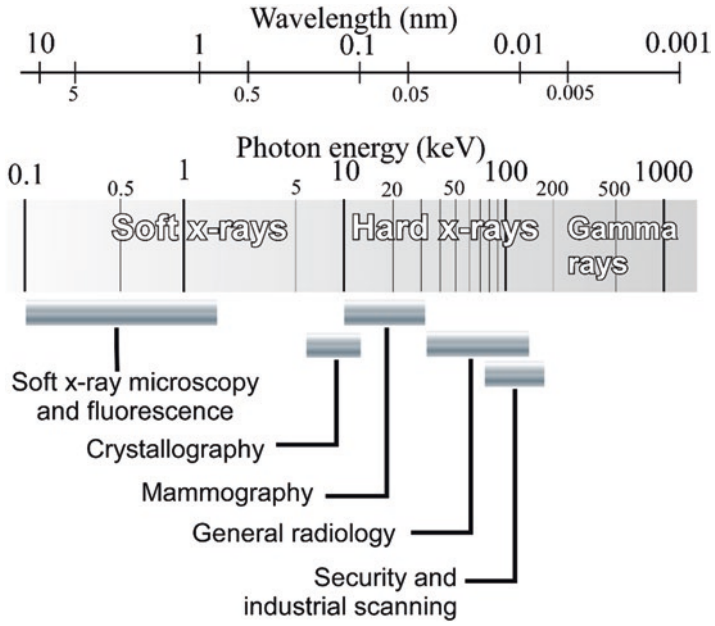

Fig. 1.1 The X-ray spectrum and applications over various spectral regions. (Idea from Ref. [1])

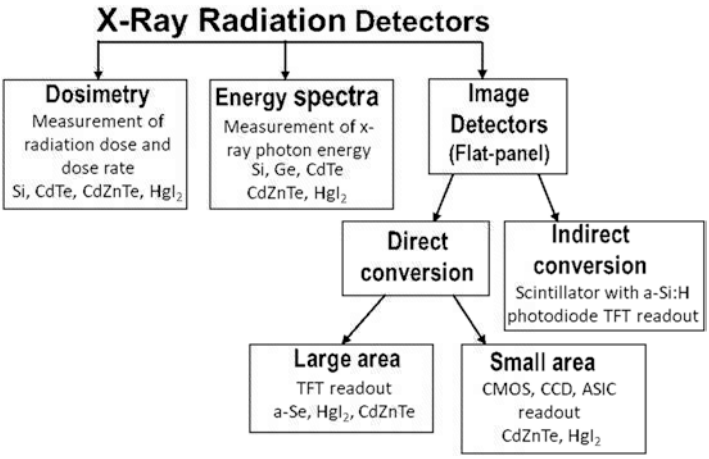

Fig. 1.2 A simplified classification of X-ray radiation detectors with corresponding photoconductor materials. (Idea from Ref. [2])

semiconductor X-ray detectors is shown in Fig. 1.2. Only semiconductor detectors will be discussed in this chapter.

The semiconductor detectors have one of three common configurations shown in Fig. 1.3, depending on the applications. The planar configuration (Fig. 1.3a) is the

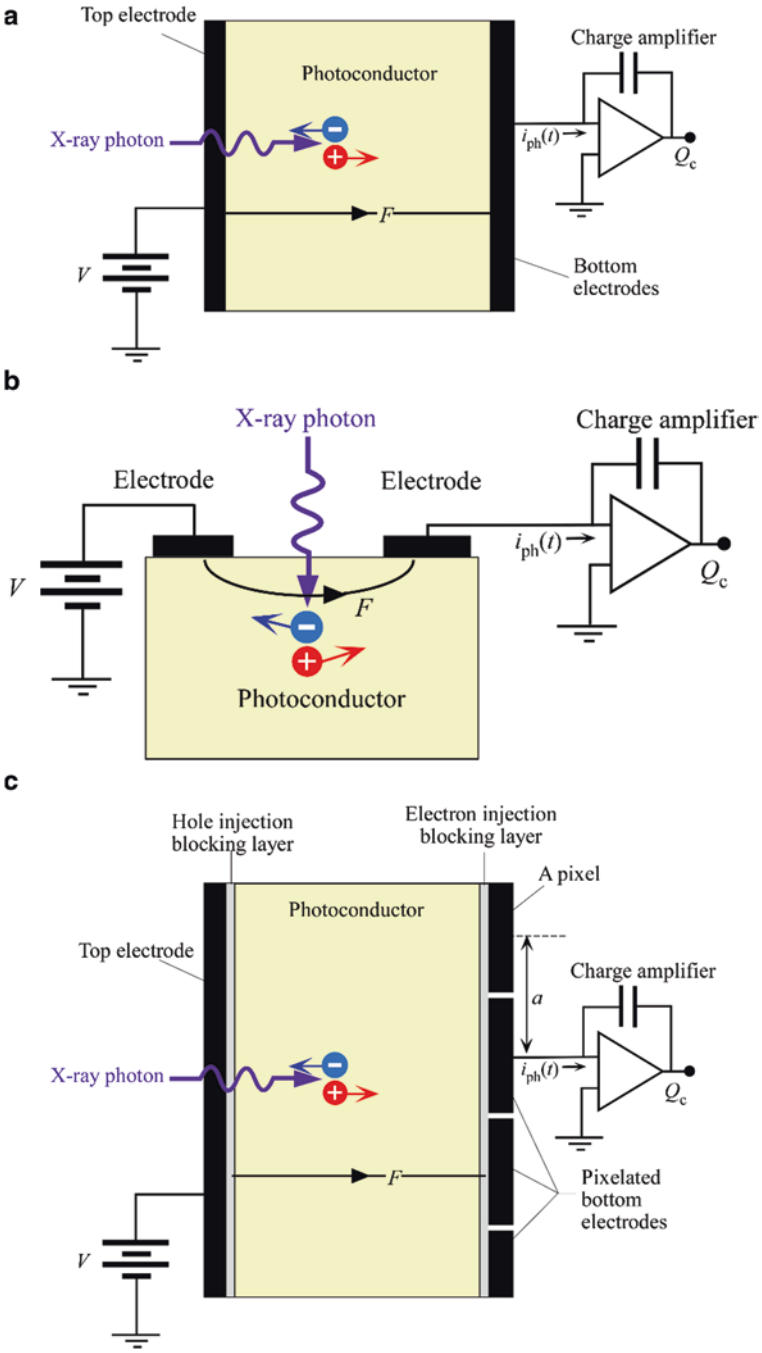

Fig. 1.3 Simplified cross-sectional structures of three basic X-ray detectors: (**a**) single element planar detector, (**b**) co-planar detector, and (**c**) pixelated detector for imaging applications. Here Q_c is the collected charge and $i_{ph}(t)$ is the instantaneous photocurrent

most common and simplest configuration for implementation, where a photoconductor layer is sandwiched between two electrodes. The co-planar configuration (Fig. 1.3b) can provide higher spectral resolution. The top electrode is a continuous metallic plate, and the bottom electrode is segmented into 2D arrays of pixels in imaging detectors (Fig. 1.3c). The photoconductor layer can have several compositions such as *p-n*, *p-i-n,* or simply metal/photoconductor/metal type. The metal/photoconductor/metal type detectors are often called photoconductive detectors. Detectors based on the *p-n* junction or a Schottky junction are reverse-biased to ensure a wider depletion layer and strong electric field in the depletion region though the field is not uniform. Therefore, *pin* devices are preferred not only because of their wider *i*-layer, or depletion layer width, but also ensuring a relatively uniform field in this depletion layer.

The top electrode is biased with a voltage source to establish a relatively uniform electric field along the photoconductor layer in the photoconductive detectors. The bulk part of the photoconductor layer used in photoconductive detectors is either intrinsic or close to intrinsic (slightly *p* or *n*-type). The X-ray absorption, ionization (EHP generation), and charge transport occur mainly in the nearly intrinsic photoconductor layer where both holes and electrons can drift by the influence of the applied electric field *F*. The X-ray generated holes and electrons drift following the electric field and induce photocurrent i_{ph} in the external circuit, which corresponds to the radiation received by the detector. An additional current, named as the dark current, continuously flows in the external circuit because of the adequate electric field in the absence of the radiation. The dark current must be as small as possible because it acts as a noise.

The detector is designed in such a way that the dark current can be minimized. There are two main sources of dark current [3, 4]: (i) thermal generation of charge carriers in the photoconductor layer and (ii) carrier injection from the contacts. The thermal generation of carrier in high bandgap semiconductors is negligibly small and its contribution to the dark current is also very small. The electrode-semiconductor contacts are blocking (e.g., Schottky junction) in nature in photoconductive detectors to minimize the carrier injection from the metallic contacts, but allow photogenerated charge carrier flow from the photoconductor layer to the electrodes to eliminate carrier accumulation at the interfaces. A very thin blocking layer is often inserted between the bulk photoconductor layer and the electrode in order to minimize the carrier injection from the electrode as shown in Fig. 1.3c. The non-injecting blocking contacts may not require if the resistivity of the photoconductor is sufficiently high [3]. The carrier injection from the metal contacts is insignificant in reverse-biased p-n or pin detectors and the dark current is controlled by the thermal generation current in the depletion region.

The fundamental concepts related to X-ray detectors such as X-ray interaction with the solid-state materials, EHP creation mechanism, signal formation principles, general requirements, and materials for X-ray detectors are described in Sect. 1.2. Two very important applications of X-ray radiation detectors in spectroscopic and flat-panel imaging are described in Sects. 1.3 and 1.4, respectively. A brief introduction to X-ray interaction position sensitive semiconductor detector structures and their implication on charge collection are given in Sect. 1.5.

1.2 X-Ray Photoconductivity

1.2.1 X-Ray Interactions with Photoconductor

X-rays interact with the photoconductor which occurs mainly by three different mechanisms. The types of interactions are the photoelectric effect, Rayleigh scattering, and Compton scattering. The incident X-rays can be completely absorbed in the medium (photoelectric effect) or scattered (Rayleigh or Compton scattering). *Rayleigh* scattering involves an elastic (coherent) scattering of X-rays by orbital electrons. The energy of the scattered X-ray is identical to that of the incident X-ray. There is no exchange of energy from the X-ray to the medium. However, the scattered X-ray experiences a change in its trajectory relative to that of the incident X-ray, and this has an adverse effect in imaging detectors, where the detection of scattered X-rays is undesirable. However, this type of interaction has a low probability of occurrence in the diagnostic X-rays. In general, the average scattering angle decreases with increasing incident X-ray energy E.

Compton scattering involves an inelastic (incoherent) scattering of an X-ray photon by an atomic electron. Compton scattering typically occurs when the energy of the X-ray photon is much greater than the binding energy of the atomic electron. Therefore, the Compton effect occurs with the outer-shell electrons. This interaction includes an electron of kinetic energy E'', an ionized atom, and a scattered X-ray photon of energy E' that is lower than the incident photon energy E. Thus, some energy is imparted to the medium in Compton scatting event. The imparted energy depends on the scattering angle which is random. The probability of Compton absorption per unit mass is approximately proportional to $E^{-0.5}$ [5].

In photoelectric interaction, the incident X-ray interacts with an orbital electron in the atom, and all its energy is transferred to the electron. Part of this energy is used to overcome the binding energy of the electron, and the remaining fraction becomes the kinetic energy E_k of the photoelectron. If the energy of the incident X-ray is higher than the binding energy of the electron, the electron is removed from its shell and a vacancy is created in that shell. The ejected electron is most likely one whose binding energy is closest to, but less than, the incident photon energy. For example, for photons whose energies exceed the K-shell binding energy, photoelectric interactions with K-shell electrons are most probable. The binding energy associated with the K-shell is called the *K-edge* and so on. This vacancy is usually filled by an electron from an outer shell, leaving a vacancy in the outer shell that in turn may be filled by an electron transition from a more distant shell. This series of transitions is called an electron cascade. The energy released by each transition is equal to the difference in binding energy between the original and final shells of the electron. This energy may be released by the atom as characteristic X-rays or Auger electrons. The probability of photoelectric absorption per unit mass is approximately proportional to Z^4/E^3, where Z is the atomic number. Emissions from transitions exceeding 100 eV are called *characteristic* or *fluorescent* X-rays. The *characteristics* X-rays are named as K-fluorescent, L-fluorescent, etc. based on the electron receiving shell.

1.2.2 Ionization Energy and Signal Formation

Energetic primary electrons created by photoelectric effect or Compton scattering travel in the solid can cause ionization along its track and create many electron-hole pairs (EHPs). As a result, a single X-ray photon can create thousands of EHPs. However, on average, a certain portion of X-ray photon energy is not absorbed in the medium because of various scattering events. The average energy absorbed in the medium by the primary X-ray interaction can be determined and is described by the linear attenuation coefficient α and energy absorption coefficient α_{en}. Thus, $(\alpha_{en}/\alpha)E$ is the average absorbed energy E_{ab} by the primary X-ray interaction per attenuated X-ray photon of energy E. For sufficiently thick medium, the escaped radiations from the primary interaction site can interact with atomic electrons of the medium like primary X-rays but at different points. Therefore, the actual average absorbed energy per attenuated X-ray photon of energy E in a very thick detector is higher than $(\alpha_{en}/\alpha)E$ and closer to E.

The average number of EHP creation per absorbed photon,

$$N_i = \frac{E_{ab}}{W_i} \tag{1.1}$$

Where W_i is the ionization energy of the medium, which is the average absorbed energy required to create a single EHP. In this case, the maximum collected charge in the external circuit would be $Q_i = eN_i$ if there is no loss of charge carriers in the detector, where e is the elementary charge. Klein [6] developed a formula to calculate the ionization energy, which is,

$$W_0 \approx CE_g + E_{phonon} \tag{1.2}$$

where E_g is the bandgap energy, C = 2.8 and 2.2 for crystalline and amorphous semiconductors, respectively, [6, 7]. Here $E_{phonon} = m\hbar\omega_p$, where m is the average number of optical phonon emission per ionization and $\hbar\omega_p$ is the optical phonon energy. The value of E_{phonon} is in the range of 0.1–0.5 eV. Note that the ionization energy obtained from Klein's formula is denoted by W_0. In most semiconductors, the ionization energy follows Eq. (1.2) and thus $W_i \approx W_0$. However, there are few exceptional semiconductors (e.g., amorphous selenium, a-Se) where the actual ionization energy $W_i >> W_0$ and depends on the electric field and photon energy [8–10]. In those cases, the Klein's formula serves as the lowest theoretical limit for the ionization energy [11].

Since the photoconductors have relatively higher resistivity and thus there is inadequate reservoir of free carriers available to surround the photogenerated carriers and maintain local charge neutrality within the time scale of interest, the photogenerated drifting carriers instantaneously induce charges at the electrodes. The rate of change of this induced charge creates current in the external circuit. Therefore, the currents resulting from the photogeneration of mobile carriers into the

photoconductive detector are due entirely to induction. The Shockley-Ramo's theorem provides a convenient way to calculate the induced current flowing through an electrode of multielectrode detectors (e.g., pixelated image detector) due to the motion of charge carriers in the detector (Fig. 1.4). The induced current I_j and charge Φ_j on an electrode j by a moving elementary positive charge e at x are given by [12–14],

$$I_j = e\boldsymbol{v}\cdot\boldsymbol{F}_{wj}(x) \tag{1.3}$$

$$\Phi_j = -eV_{wj}(x) \tag{1.4}$$

where v is the instantaneous velocity of charge e, $F_{wj}(x)$ and $V_{wj}(x)$ are the weighting field and potential of electrode j. $F_{wj}(x)$ and $V_{wj}(x)$ are the electric field and potential that would exist at charge e's instantaneous position x if the electrode of interest (j) is raised to unit potential and all other electrodes kept at zero potential and all charges removed. V_{wj} is unitless and the unit of F_{wj} is m^{-1}. An analytical expression for the weighting potential in pixelated detectors having finite square pixels has been derived in literature [15].

Let a positive point charge be moving from x_1 to x_2. Φ_{j1} and Φ_{j2} are the induced charges at electrode j when the charge is at x_1 and x_2, respectively. The induced charges, $\Phi_{j1} = -eV_{wj}(x_1)$ and $\Phi_{j2} = -eV_{wj}(x_2)$. The collected charge at electrode j for moving a positive point charge from x_1 to x_2 is given by,

$$Q_j = -\left(\Phi_{j2} - \Phi_{j1}\right) = e\left[V_{wj}(x_2) - V_{wj}(x_1)\right] \tag{1.5}$$

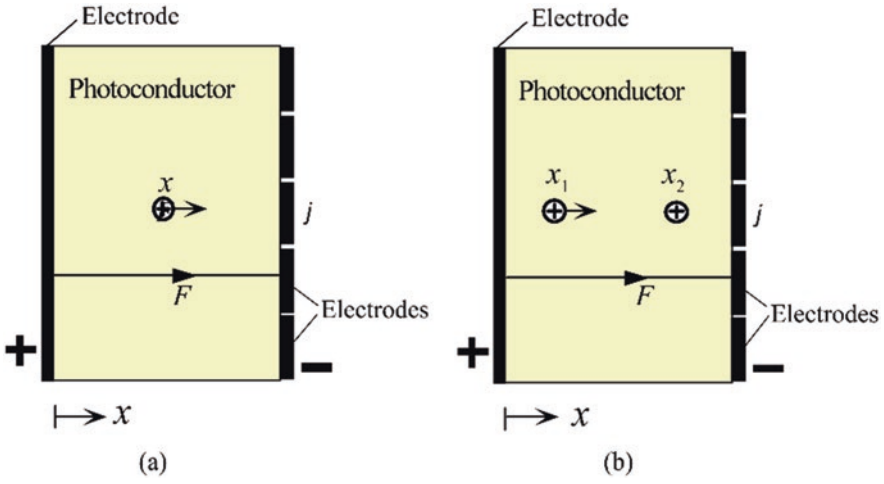

Fig. 1.4 A cross section of a multielectrode detector: (**a**) an elementary positive charge at x is drifting by an applied field F. (**b**) An elementary positive charge is moved from point x_1 to x_2

For a large area single-element detector, $F_w(x) = 1/L$, $V_w(x) = x/L$, and thus current, $i = ev/L$ [16], where L is the photoconductor thickness. In this case, the collected charge at the electrode for moving a positive point charge from x_1 to x_2 is simply,

$$Q_j = -\left(\Phi_{j2} - \Phi_{j1}\right) = e\frac{\left(x_2 - x_1\right)}{L} \tag{1.6}$$

If there is carrier trapping, only a fraction of photogenerated charge is collected in the external circuit. Consider an electron and a hole (an EHP) are generated at x and drift under the influence of the electric field. The average electron and hole photocurrents are $i_e(t) = (ev_e/L)\exp(-t/\tau_e)$ for $t < t_e$ and $i_h(t) = (ev_h/L)\exp(-t/\tau_h)$ for $t < t_h$, respectively; where $v_e = \mu_e F$, $v_h = \mu_h F$, $t_e = x/v_e$, $t_e = (L - x)/v_h$, μ is the carrier mobility, and τ is the carrier lifetime. The subscripts e and h on μ and τ refer to electrons and holes, respectively. Both types of carrier drifts produce currents of the same polarity at any electrode. Therefore, the collected charge at any electrode is the sum of the contributions of both types of carrier transports. The average collected charge for applying a positive bias at the top electrode (the electric field is along the positive x direction) is,

$$\begin{aligned} Q_c(x) &= \int_0^{t_e} i_e(t)\,\mathrm{d}t + \int_0^{t_h} i_h(t)\,\mathrm{d}t \\ &= \frac{e\mu_e\tau_e F}{L}\left[1 - e^{-x/\mu_e\tau_e F}\right] + \frac{e\mu_h\tau_h F}{L}\left[1 - e^{-(L-x)/\mu_h\tau_h F}\right] \end{aligned} \tag{1.7}$$

where $t_e = x/\mu_e F$ and $t_h = (L - x)/\mu_h F$ are the electron and hole transit times, respectively. Eq. (1.7) is the well-known *Hecht equation* for calculating the average collected charge. The maximum collected charge, $Q_c = e$, when the lifetime of both holes and electrons is infinity. Therefore, the charge collection efficiency,

$$\eta_{cc}(x) = \frac{\mu_e\tau_e F}{L}\left[1 - e^{-x/\mu_e\tau_e F}\right] + \frac{\mu_h\tau_h F}{L}\left[1 - e^{-(L-x)/\mu_h\tau_h F}\right] \tag{1.8}$$

Equation (1.8) is the charge collection efficiency for a free EHP generation at x, which depends not only on the charge carriers transport properties (mobility-lifetime of both holes and electrons) and electric field, but also on the location where the charge is created. For exponential absorption throughout the photoconductor layer (which is the case for X-rays), the average charge collection efficiency [17, 18],

$$\eta_{cc} = x_h\left[1 + \frac{\left(e^{-1/x_h} - e^{-1/\Delta}\right)}{\left(\Delta/x_h - 1\right)\eta}\right] + x_e\left[1 - \frac{\left(1 - e^{-1/\Delta - 1/x_e}\right)}{\left(\Delta/x_e + 1\right)\eta}\right], \tag{1.9}$$

where $x_e = \mu_e \tau_e F/L$, $x_h = \mu_h \tau_h F/L$, $\Delta = 1/\alpha L$ and $\eta = 1 - \exp(-1/\Delta)$ is the quantum efficiency of the photoconductive detector. Therefore, the actual collected charge $Q_c = Q_i \eta \eta_{cc}$, where Q_i is the X-ray generated free charges, η accounts for the average fraction of the X-rays that are attenuated within the photoconductor thickness. Though Eq. (1.9) applies under small signal conditions under uniform electric field, the equation shows much resilience even under strong injection and errors are not as large as one may anticipate [19]. Further, Eq. (1.9) assumes that the carrier transport properties (i.e., $\mu\tau$ do not vary across the sample). It is still possible to use Eq. (1.9) in cases where the carrier ranges are not uniform in the sample by suitably defining effective carrier ranges as discussed in [18]. The charge collection efficiency for a given photoconductor depends on x_e and x_h and hence on the applied field. Most semiconductors have asymmetric $\mu\tau$ products. Ensuring that the carrier with the longer range is drifted towards the bottom electrode can provide a better charge collection efficiency [15].

1.2.3 X-Ray Photoconductors

The following are the general properties of the X-ray photoconductor [20] used in X-ray detectors:

1. Most of the incident X-ray radiation should be absorbed within a practical photoconductor thickness. This means that, over the energy range of interest, the attenuation depth δ (inverse of the attenuation coefficent α of the photoconductor) of the X-rays must be substantially less than the photoconductor layer thickness L. Higher atomic number materials give higher attenuation.
2. The photoconductor should have high intrinsic X-ray sensitivity, i.e., it must be able to generate as many collectable (free) EHPs as possible per unit of incident radiation. This means the ionization energy, W_i, (amount of radiation energy required to create a single free EHP) must be as low as possible.
3. The photoconductor should have good charge carrier transport properties. That means the product of carrier drift mobility (μ) and carrier lifetime (τ) should be high so that the charge collection efficiency is close to unity.
4. The properties of the photoconductor should not change with time because of repeated exposure to X-rays, i.e., X-ray fatigue and X-ray damage should be negligible.
5. The detector should preferably operate at around room temperature.

Both elementary (Si, Ge, or Se) and compound semiconductors are used in radiation detectors. Si detectors are used for low energy X-rays (<30 keV) [21]. They are mechanically and chemically robust. High purity Ge detectors have high resolution and efficiency for detection of hard X-rays. Both Si and Ge detectors often need to operate at low ambient temperature to decrease the dark current from thermally generated charge carriers [22]. Compound semiconductors are mostly derived from

groups III and V (e.g., GaAs, GaN, InP) and groups II and VI (e.g., CdTe) of the periodic table. The compound semiconductors have few distinct advantages as their electronic and chemical properties can be modified by band-gap engineering for specific applications in radiation detectors. For example, adding a few percent Zn into the CdTe lattice strengthens the lattice of CdTe, increases the band gap [23], decreases the conductivity, and hence reduces the dark current. A few selected compound semiconductors such as CdTe, CdZnTe ($Cd_{0.92}Zn_{0.08}Te$ – $Cd_{0.9}Zn_{0.1}Te$), and HgI_2 are already used in commercial X-ray and γ-ray spectroscopic detectors. They do not need cooling and can be used at room temperature, which is a distinct advantage. Their properties have been extensively reviewed in the literature [21, 22, 24–29] and in recent book [3] and chapters [30, 31]. A comprehensive description of the photoconductors for large area medical X-ray image detectors can be found in Refs. [32, 33].

Group II-VI materials attract special attention for radiation detectors because they can provide continuous broad range of bandgaps (e.g., 0.15 eV for HgTe to 4.4 eV for MgS). These compounds are formed by combining a Group IIb metal (such as Zn, Cd, and Hg) with a Group VIa cation (usually S, Se or Te). They have high effective Z and thus provide high stopping power (i.e., high attenuation). The high stopping power enables thinner detector. All II-VI binaries have direct bandgaps. The typical main compounds are CdTe and HgTe. They are alloyed with Zn, Se, Mn, or Cd to create ternary compounds (e.g., $Cd_{(1-x)}Zn_xTe$, $Cd_{(1-x)}Mn_xTe$ and $Hg_{(1-x)}Cd_xTe$) for commercial radiation detectors. Group II-VI semiconductors can also be created in quaternary forms, although less common than III-V varieties.

There are many experimental semiconductors that have good commercial potential. For example, GaAs *p-i-n* X-ray detectors for spectroscopy have been demonstrated [34]. GaAs arrays have been also demonstrated for X-ray spectroscopy with high resolution [35]. SiC is another possible X-ray detector material that has favorable properties for X-ray spectrum measurements and can be used in harsh environments [36, 37]. GaN-based X-ray radiation detectors are more suitable at high temperature and high radiation field operation [38, 39]. The electronic properties of typical materials used in dosimetry and spectroscopic detectors are summarized in Table 1.1. The materials for imaging detectors are described in Sect. 1.4.

1.3 X-Ray Spectroscopic Detectors

The measurement of the energy distribution of the incident radiation is known as radiation spectroscopy. The basic principle of spectroscopy measurement set up using a semiconductor detector is illustrated in Fig. 1.5. The fundamental properties of a radiation detector are often determined by its pulse height spectrum. To construct a pulse height spectrum, a stream of monoenergetic photons is irradiated within the detector. Photons are sufficiently separated so that one photon at a time is absorbed and the collected charges from the individual photons can be separately processed and stored in the multichannel analyzer. The preamplifier integrates the

Table 1.1 Selected examples of *single crystal* semiconductors for use in X-ray detectors for the measurement of dose or energy spectra. If the detector type is not fully known, metal/semiconductor/metal is shown. HPGe is high purity Ge

Semi-conductor	Detector type	Density (g cm^{-3})	E_g (eV)	W_i (eV)	F_N	Typical mobility-lifetime
Si	*pn*, *pin* or Schottky junction	2.33	1.12	3.62	0.08–0.13	$\mu_e\tau_e \approx 1$ cm^2/V, $\mu_h\tau_h \approx 1$ cm^2/V
Ge Ge (Li)	*pin*-like, metal/HPGe/metal	5.33	0.72	2.96	0.06–0.11	$\mu_e\tau_e \approx 1$ cm^2/V, $\mu_h\tau_h \approx 1$ cm^2/V
GaAs	*pin*	5.32	1.43	4.18	0.14	$\mu_e\tau_e \approx 10^{-4}$ cm^2/V, $\mu_h\tau_h \approx 4 \times 10^{-6}$ cm^2/V
CdTe	Schottky, *pin*, and metal/CdTe/metal	5.85	1.44	4.43	0.06–0.09	$\mu_e\tau_e \approx 10^{-3}$ cm^2/V, $\mu_h\tau_h \approx 10^{-4}$ cm^2/V
CdZnTe	Schottky, *pin*, and metal/CdTe/metal	5.8	1.57	4.6	0.10	$\mu_e\tau_e \approx 10^{-3}$ cm^2/V, $\mu_h\tau_h \approx 10^{-4}$ cm^2/V
HgI_2	Metal/HgI_2/metal	6.4	2.15	4.2	0.12	$\mu_e\tau_e \approx 3 \times 10^{-4}$ cm^2/V, $\mu_h\tau_h \approx 4 \times 10^{-5}$ cm^2/V
4H-SiC	Metal/HgI_2/metal	3.29	3.27	7.28	0.128	$\mu_e\tau_e \approx 4 \times 10^{-4}$ cm^2/V, $\mu_h\tau_h \approx 8 \times 10^{-5}$ cm^2/V
InP	Metal/InP/metal	4.79	1.34	4.2	0.13	$\mu_e\tau_e \approx 2 \times 10^{-5}$ cm^2/V, $\mu_h\tau_h \approx 10^{-5}$ cm^2/V

Source: Data are typical values quoted in the literature as in Refs. [3, 28]

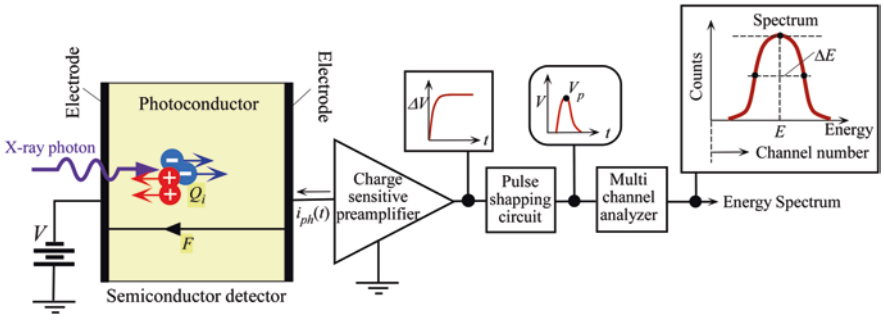

Fig. 1.5 The basic principle of photon energy spectrum measurements using a semiconductor detector

transient current pulse to produce a voltage step ΔV proportional to collected Q_c. The pulse shaping circuit converts the preamplifier output signal into a form suitable for measurements, producing an output voltage pulse with pulse height V_p proportional to Q_c. However, a statistical variation in Q_c is observed for different incident photons and so does in voltage pulse height V_p. The multichannel analyzer sorts out incoming voltage pulses according to their output pulse height and stores the number of pulses (count) of a particular charge level (channel number). We can

suitably calibrate the measurement system for a known photon energy so that we can convert the Q_c to photon energy E and plot the number of occurrences (counts) against the photon energy E which is called a pulse height spectrum. The detailed analyses of the various components of spectroscopic measurement technique are described in radiation detection and measurement textbooks such as in references [40, 41]. In the ideal case, we would find a Gaussian distribution with a mean that corresponds to E and a full width between half maximum (FWHM), ΔE. If σ is the standard deviation of the Gaussian profile, then $\Delta E = 2.35\sigma$.

There are several potential sources of fluctuation for the observed ΔE. These include any drift of the operating characteristics of the detector during the measurements, sources of random noise within the detector and instrumentation system (electronic noise), and statistical noise arising from the discrete nature of the measured signal itself. The third source represents the minimum amount of fluctuation that will always be present in the detector signal, which sets an important limit on detector performance.

The overall observed variance can be written as

$$\sigma^2 = \sigma_{\text{con}}^2 + \sigma_{\text{cc}}^2 + \sigma_e^2, \tag{1.10}$$

Where σ_{con} is the standard deviation owing to carrier generation, σ_{cc} is the standard deviation owing to incomplete charge collection, and σ_e is the standard deviation owing to leakage current and amplifier noise. The electronic noise is a lumped value incorporating the noise associated with the leakage current of the detector and the noise due to the electronic chain, starting with the preamplifier, to the final output.

As mentioned earlier, the energy transfer of an X-ray photon energy to the matter occurs through the creation of an energetic primary electron. This energetic primary electron slows down by transferring energy in a cascade of energy transfer processes to electrons and the lattice. The conversion process of an absorbed photon to the number of carriers has fluctuations about its mean value N_i due to the randomness of this whole processes. If the conversion (the ionization of the medium by the primary electron) was a string of independent events, the conversion statistics would be a Poisson distribution so that the variance of the conversion process would be N_i. In fact, the energy conversion events are correlated by energy conservation. Therefore, the variance in the number of charge carrier generation is modified by a Fano factor F_N [42], and thus the actual variance of conversion is $F_N N_i$. If ΔE_{con} is the FWHM in the pulse height spectrum in Fig. 1.5 from the statistics of the conversion process alone, then this would be

$$\Delta E_{\text{con}} = 2.355\sqrt{F_N E W_i} \tag{1.11}$$

The Fano factors for many semiconductors are typically less than 1 and are listed in Table 1.1. $F_N < 1$ is accounted by the fact that the spread in the collected number of carriers is less than that expected from Poisson statistics. A reliable experimental measurement of F_N requires that the photogenerated carriers suffer no trapping (all

are collected) and the electronic noise in the measurement circuit is suppressed. Fano factor also has temperature and photon energy dependence [3].

The second important broadening mechanism is the effect of charge carrier trapping during the drift of the carriers towards their collection electrodes. Some of charge carriers can be trapped during their drift towards the electrodes and are not fully collected, so the measured charge is less than Q_i. There are two intermingled fluctuations in charge collection. First is that not every photon is absorbed at x, so there will be fluctuations in x and hence in Q_c. The absorption probability of a photon along the sample follows an exponential distribution $\exp(-\alpha x)$ where α is the linear attenuation coefficient of the medium. The variance of charge collection efficiency for the fluctuation on interaction distance x can be found in Ref. [43, 44]. Second, charge carrier trapping during drift is a stochastic process and there will be fluctuations in η_{cc} even if each photon was absorbed exactly at x. The signal variance for the fluctuation in η_{cc} owing to charge carrier trapping for photon interaction at x is given in Ref. [45].

The resolution of a spectroscopic detectors is nominally quoted in terms of the FWHM width ΔE at the photon energy E. Obviously, the smaller is ΔE, the better is the resolution of the detector in discriminating different energy photons. High purity Ge detectors operated at low temperatures have especially high spectral resolution. For example, if the electronic noise can be reduced by special techniques, then a resolution of 345 eV at 59.5 keV or 0.57% is achievable at 100 K [46], though typical quoted values in various tables have been 670 eV at 77 K [3]. Typically, the energy resolution with compound semiconductor detectors at room temperature is approximately 2% or more, but less at low temperatures as discussed in references [28]. Tables 9.5, 4, and 3 in references [3, 26, 28], respectively, provide the best values that are observed for a range of semiconductors at energies 5.9 keV and 59.5 keV.

1.4 Flat-Panel X-Ray Image Detectors

1.4.1 Materials and Structures

The flat-panel X-ray imagers (FPXIs) are, at present, the most successful digital X-ray detectors for screening medical imaging such as mammography and general radiography [47–50]. The last few decades have seen a nearly full transformation of X-ray imaging to modern digital imaging. Digital X-ray image sensors have two major parts; the detector where X-rays are absorbed and charge carriers are generated and collected, and the peripheral electronics (including a two-dimensional active-matrix arrays, AMA) that scan and process the collected charge from the detector for display or other form of readable information [51]. An AMA is a two-dimensional large array of pixels as shown in Fig. 1.6. The requirements on the digital detector technology have become more and more demanding as medical X-ray imaging today is not only about projection imaging, but involves real-time imaging

(fluoroscopy) and tomosynthesis, among other imaging enhancements such as dual energy imaging, photon counting, etc., each of which has its own demands on the detector technology [52–58]. The FPXIs are generally either phosphor-based (indirect conversion) or photoconductor-based (direct conversion). In indirect method, X-ray energy is converted into light photons in phosphor layer (mostly cesium iodide, CsI) and these light photons are then detected by a photodiode. In direct method, X-ray photons directly generate EHPs in the photoconductor layer, which are collected on electrodes. The typical single pixel structures of both direct and indirect conversion FPXIs with TFT are shown in Fig. 1.7. A comprehensive and detailed review of flat-panel image detectors, both direct and indirect, has been given by Rowlands and Yorkston [59]. A drawback of indirect method is that the light photons are scattered and blur the image. The direct conversion detectors produce much sharper images than the indirect conversion detectors [48]. The focus of this section is on the properties and the performance of direct conversion X-ray image detectors.

For large area detectors, each pixel has a thin film transistor (TFT) and a charge storage capacitance. The TFT gate (G) is for the control of the "on" or "off" state of the TFT and connected to a particular address line *i,* the drain (D) is connected to a pixel electrode and a pixel storage capacitor, the source is connected to a particular data line *j*. The AMA has $M \times N$ number of gate and data lines, where M and N can be several thousand. The intrinsic read-out resolution of the detector is determined by the pixel pitch, which is typically 50–100 μm. The TFT array is laid out on a suitable flat rectangular glass substrate and is purchased by the detector manufacturing company as a component onto which the semiconducting photoconductor is coated. The TFT-AMA substrate makes use of the well-established hydrogenated amorphous silicon (*a*-Si:H) technology for displays. A photoconductive layer is deposited on top of the AMA substrate (Fig. 1.7). A suitable electrode is deposited on the top surface to apply a bias voltage, which establishes a field in the photoconductor. Upon absorption of X-ray photons through the top surface, electrons and holes are generated in the photoconductor layer and these carriers drift and give rise to an X-ray photocurrent. Each pixel stores an amount charge in the storage capacitor based on the radiation received on top of that pixel. The stored charge from the capacitors can be read through properly addressing the TFT (*i*,*j*) via the gate (*i*) and source (*j*) lines. The electrical signals from pixels are amplified, multiplexed, and digitized so that the image can be conveniently displayed in a computer screen. The signal scanning technique is adequately described in these Refs. [51, 59, 60].

In the case of small area imaging detectors, the TFT in AMA can be replaced by CMOS, CCD or, a particular ASIC (Application Specific Integrated Circuit) pixelated read-out chip. For direct conversion detectors, an X-ray photoconductor such as CdZnTe crystals are usually indium bump-bonded (equivalent to "cold welding") to electrodes on a CMOS [61]. CdZnTe crystals have also been bonded to ASIC read-out chips and CCDs using indium bumps to produce high resolution detectors for slot scanning X-ray imaging [62, 63]. Direct coating of the CMOS with a photoconductor has also been tried, for example, *a*-Se directly evaporated onto a defined area of the CMOS [64]. In recent years, advances have been made in increasing the

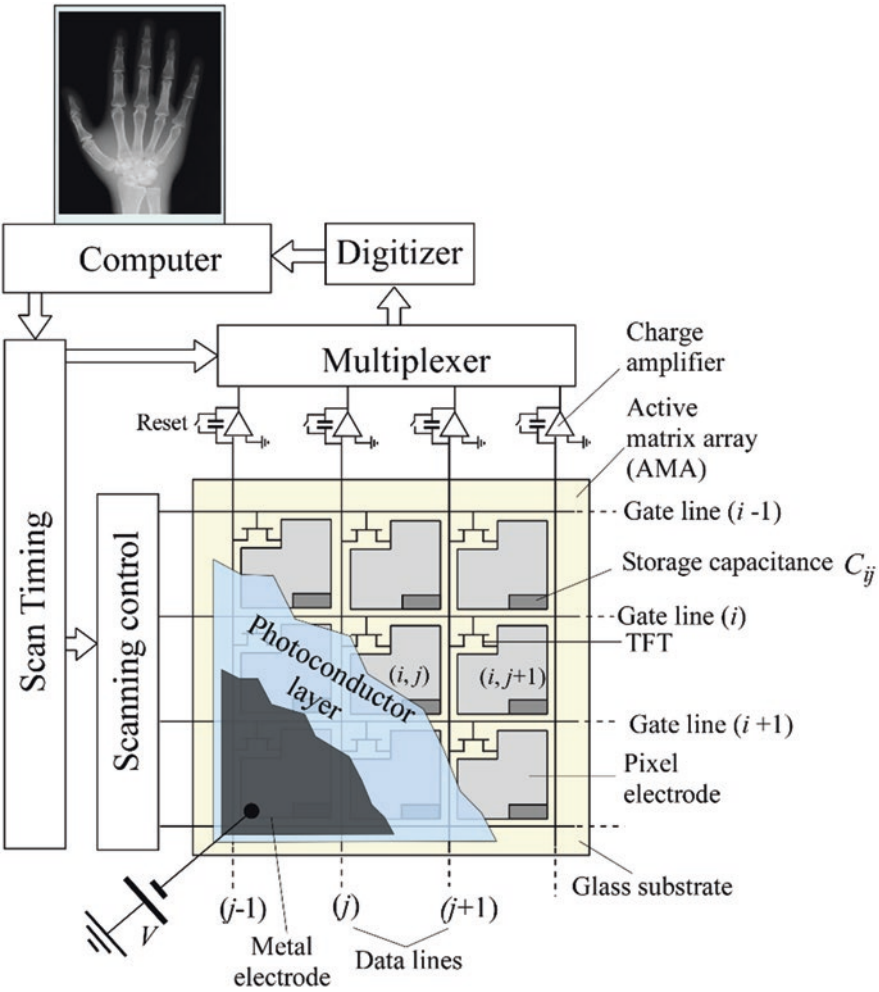

Fig. 1.6 The structure of a typical direct conversion active-matrix array-based flat panel X-ray imager. (Idea from Ref. [51])

effective imaging area of wafer-size CMOS chips through stitching and tiling [65]. In another application, polycrystalline layer of HgI_2 was grown directly on a CMOS chip (10 cm × 10 cm) to construct an X-ray imager [66]. There are several distinct advantages to using crystalline photoconductors on CMOS read-out chips. First is that the pixel size can be made very small and the whole operation can be very fast compared to TFT arrays. The second is that most CMOS imaging chips have on-pixel MOS transistors that provide on-pixel amplification to improve the imaging performances. Presently, the largest area commercial CMOS sensors are about 11 cm × 14 cm and use indirect conversion as described in [67]. Manufacturers such as Dexela and Teledyne-DALSA also offer CMOS-tiled detectors for specific X-ray

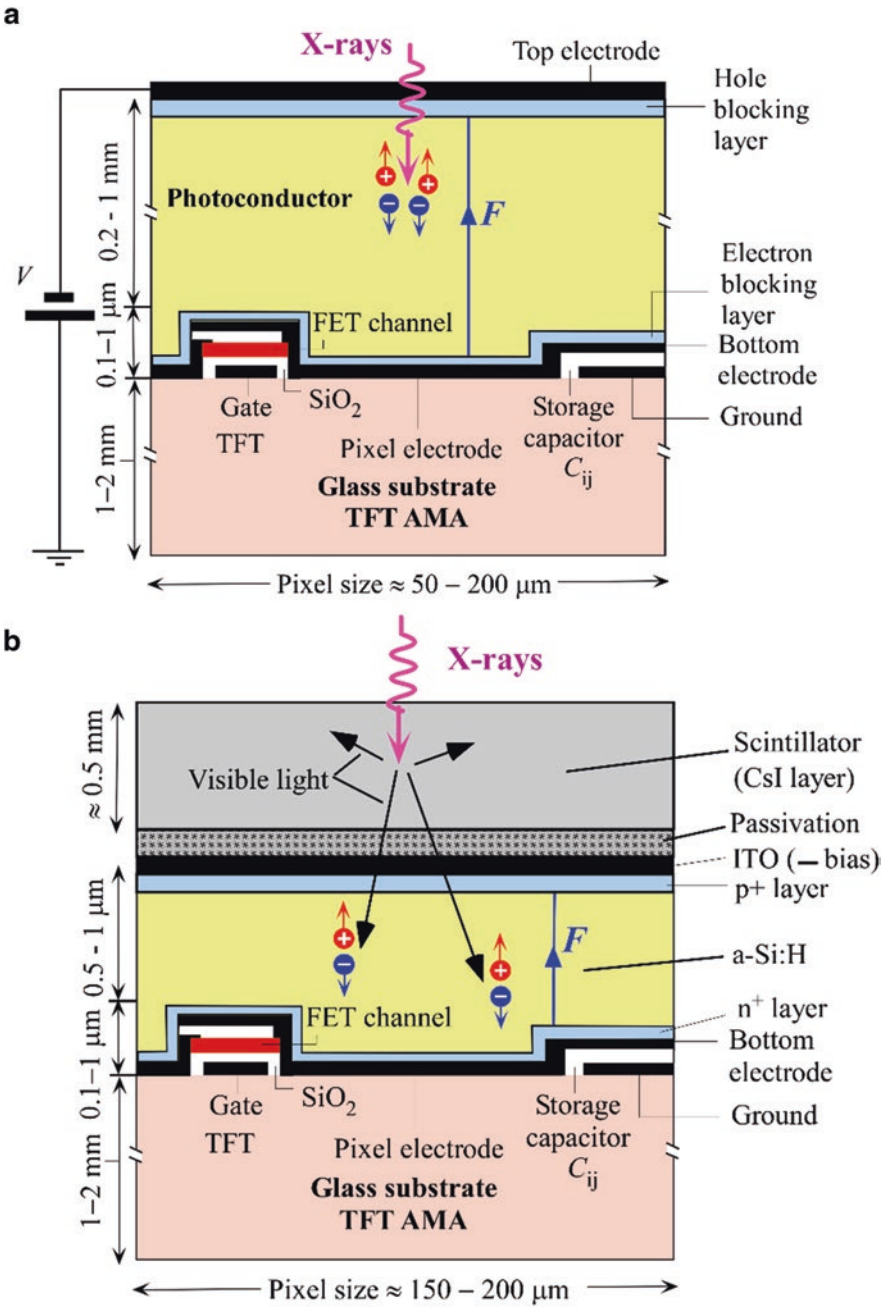

Fig. 1.7 A typical pixel structure of the TFT-based flat-panel detector: (**a**) a pixel element of the direct conversion FPXI, and (**b**) a pixel element of the indirect conversion FPXI

imaging applications that include not only medical imaging but also industrial imaging (e.g., nondestructive testing).

Stabilized *a*-Se is currently the only photoconductor for large area commercial X-ray image sensors, especially for mammography [51, 68]. Stabilized means that *a*-Se has been alloyed with 0.2–0.5%. As to prevent the crystallization of pure a-Se and then doped with Cl in the ppm amounts to control the charge transport (see [69] and recent review in [70]). The commercial *a*-Se detector is *n-i-p* or *p-i-n* type, where bulk *i*-layer is the stabilized *a*-Se layer [5]. These *p*-like and *n*-like layers do not have conventional *p*- or *n*-layer definitions in crystalline semiconductor theory based on electron and hole concentrations or the position of the Fermi level, rather they have a very high concentration of deep trap centers for oppositely charged carriers. In the *p*-like layer, the holes are relatively mobile, but electrons get easily trapped, and similarly in the *n*-like layer, electrons are mobile, but the holes get trapped easily. The thickness of these *p*- or *n*-like layers is few microns, whereas the *i*-layer thickness is at least few hundred microns. The thin *p*- or *n*-like layers act as "blocking layers". The trapped charge carriers in these blocking layers reduce the electric field at the contacts and, hence, reduce the carrier injection from the electrodes, which reduces the dark current [71]. The *p-i-n* structure was the key to the success of the *a*-Se-based FPXI because it allowed the dark current to be extinguished to an innocuous level [72–74].

A-Se is the most preferred photoconductor for direct-conversion X-ray detectors because of its low dark current, convenient low-temperature deposition over a large area, and good charge-transport properties. There is one remarkable drawback of *a*-Se, which is its lower intrinsic X-ray sensitivity (i.e., large W_i) ionization energy as compared to its competitors, such as polycrystalline HgI_2 or CdZnTe [32]. For example, the typical value of the electric field used in *a*-Se detectors is 10 V/μm where the value of W_i is about 45 eV; the value of W_i is 5–6 eV for polycrystalline mercuric iodide (poly-HgI_2) and poly-CdZnTe. The imaging properties of *a*-Se based FPXIs for various medical imaging modalities have been well-examined and analyzed; see for example [75–80]. There have been a number of other photoconductors, such as polycrystalline layers of TlBr [81, 82], PbI_2 [83–86], HgI_2 [60, 87–91], CdTe [92], CdZnTe [93, 94], PbO [95–98], and various hybrid organic–inorganic perovskite (e.g., methylammonium lead halides, MA Pb-halides) [99–105] that have been investigated to replace *a*-Se. Some of these, particularly HgI_2 and $MAPbI_3$ [60, 106], have shown much potential for use in commercial FPXI applications. MA Pb-halide perovskites, in polycrystalline form, can be easily and cheaply prepared in large areas from solution (in contrast to vacuum deposition) and have already shown very good performance in photovoltaics and photodetector applications [107, 108]. The basic underlying problem with most of these semiconductors is that they exhibit either an unacceptably large dark current under high fields needed to extract all X-ray generated charges or they possess significantly incomplete charge collection, and its consequences such as low resolution and image lag because they need to be operated at a low field to prevent a large dark current [32, 51]. Another drawback of polycrystalline materials is the adverse effects of grain boundaries in limiting charge transport and the nonuniform response